Robust Optical Wireless Link for the Backhaul and Fronthaul of Small Radio Cells

Dominic Schulz, Volker Jungnickel, Christos Alexakis, Michael Schlosser, Jonas Hilt, Anagnostis Paraskevopoulos, Liane Grobe, Péter Farkas, and Ronald Freund

(Invited Paper)

***Abstract*—This paper summarizes recent work on the use of optical wireless links as a robust outdoor backhaul solution for small radio cells, such as WiFi, LTE and 5G, over distances between 20 and 200 m. Results of a 5-month outdoor field trial in Berlin, Germany, indicate that the visibility range was never below 180 m, with more than 1 km in 99% of all times during this period. Rate-adaptive transmission proved to improve the availability remarkably in the occasional presence of fog or sunlight. A mathematical model of the backhaul link including these impairments is presented and implemented to obtain an optimized link design. A prototype was realized, accordingly, using low-cost optoelectronic components and a 1 Gb/s baseband chipset. Gross data rates of 800, 500, and 225 Mb/s have been achieved in real-time operation over 20, 100, and 215 m outdoor link distance, respectively, with 2 ms latency at 95% load. Finally, we discuss further evolution towards 5G mobile networks.**

***Index Terms*—Backhaul, Fronthaul, 5G, LED, LTE, optical wireless communications, small cells.**

I. Introduction

HIGH-SPEED optical wireless communication (OWC) has many potential applications [1] as shown in Fig. 1. Radio is more often used, because it bridges longer distances more easily. OWC offers several terahertz of additional, unlicensed bandwidth, as a possible relief for radio spectrum, which is already overcrowded due to the increasing demand for new data-hungry mobile services. The idea of offloading a fraction of the wireless traffic into the unregulated and nearly unlimited optical spectrum becomes increasingly popular, leading to so-called convergent networks in which optical and wireless links are used in a complementary manner [2].

In a mobile network, base coverage is provided in a first phase by means of a homogeneous deployment of macro-cells.

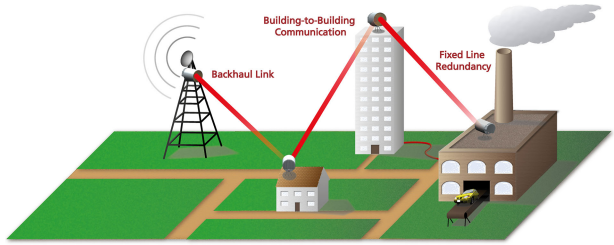

Fig. 1. Application scenario as a short-range point-to-point backhaul link.

In a second phase, a higher capacity is reached through network densification. Small mobile radio cells are added to the network at locations where the traffic density is high. With modern interference management schemes, radio spectrum can be fully reused. Each small cell offers new capacity so that more users can be served in parallel to the users already covered by the macro-cell in the same area [3]. Small cells need new links to the fixed network infrastructure. In principle, these links can be provided by a variety of technologies, either via fixed copper or fiber-optical links or wireless technologies such as micro-, mm-wave and OWC. Wireless links play a crucial role during the initial deployment of a new mobile infrastructure. They are used until the fixed link becomes available, and sometimes as a permanent solution, if, e.g., digging the fiber is too expensive.

Note the distinction between back- and fronthaul in mobile networks. While backhaul denotes the link between a base station and the core network, fronthaul is the link between the baseband unit and the remote radio head (RRH). Today, backhaul is realized using Ethernet, while fronthaul is often realized using the common public radio interface (CPRI) where samples of the baseband signal are quantized and transported over a serial link. Modern deployment concepts for mobile networks tend to centralize the baseband processing which can be located several ten kilometers away from the RRHs in the fixed network behind the radio link. In this case, fronthaul has to be transported via the fixed access infrastructure where, however, Ethernet is widely used being incompatible with CPRI.

Modern mobile technologies use more antennas and higher bandwidth, e.g., by aggregating multiple frequency bands. For this reason, fronthaul data rates tend to explode, when using current transport technologies like CPRI. Accordingly, new fronthaul technologies are currently discussed where Ethernet is used as a transport protocol and part of the baseband processing is shifted to the RRH, which is also denoted as the modified

Manuscript received October 12, 2015; revised December 15, 2015; accepted January 18, 2016. Date of current version March 3, 2016. This work was supported in part by the European Union Seventh Framework Program FP7-ICT-2011-8 in the collaborative project SODALES under grant agreement N°318600.V. Jungnickel would like to thank Wolfgang Störmer (Deutsche Telekom AG) for insightful discussions about the deployment problems related to small cells.

D. Schulz, V. Jungnickel, C. Alexakis, J. Hilt, A. Paraskevopoulos, P. Farkas, and R. Freund are with the Fraunhofer Heinrich Hertz Institute, Berlin 10587, Germany (e-mail: dominic.schulz@hhi.fraunhofer.de; volker.jungnickel@hhi.fraunhofer.de; christos.alexakis@hhi.fraunhofer.de; jonas.hilt@hhi.fraunhofer.de; anagnostis.paraskevopoulos@hhi.fraunhofer.de; peter.farkas@hhi.fraunhofer.de; ronald.freund@hhi.fraunhofer.de).

M. Schlosser is with BISDN GmbH, Berlin 10785, Germany (e-mail: michael.schlosser@bisdn.de).

L. Grobe is with P3 communications GmbH, Berlin 10713, Germany.

Color versions of one or more of the figures in this paper are available online at http://ieeexplore.ieee.org.

Digital Object Identifier 10.1109/JLT.2016.2523801

functional split. Data and some control information are then transported over Ethernet, at least in the downlink, rather than digitized waveforms, and the data rate can be reduced significantly [4], [5]. In the fourth generation (4G) of mobile networks, based on the 3GPP Long Term Evolution (LTE), small cells are usually connected via backhaul. In 5G, interference coordination becomes tighter which suggests that small cells are connected via the fronthaul. Using Ethernet and the modified functional split, fronthaul can then be realized also by using wireless technologies. This paper demonstrates that optical wireless links can be used as a low-cost backhaul solution for small cells in 4G. Moreover, the potential use as a fronthaul technology for 5G is discussed, assuming that the modified functional split is applied.

Optical wireless has a long history, starting with Graham Bell's photophone in 1880 installed over a link length of 200 m [6]. Nowadays, OWC links commonly use infrared lasers with high bandwidth operated in a transparent mode, i.e., without coding/decoding the data at the transmitter/receiver side. Eventually, a limiting amplifier followed by a clock-data recovery is used to regenerate the data signal. The advantage is that these systems are very simple and can support various protocols at ultra-low latency limited only by time-of-flight through the atmosphere. On the other hand, links can only handle impairment effects, such as sunlight, fog ($>$ 150 m), atmospheric turbulence ($>$ 500 m) [7], and clouds in satellite-to-ground links (several km), by providing a considerable link margin. If this margin proves to be insufficient under specific weather conditions, the link is interrupted.

Enhanced robustness in variable weather conditions is considered as a first important objective. In urban areas, inter-site distance between typical macro-cells is around 500 m, i.e., losses through fog and sunlight are essential. Mobile operators developed a common understanding that link availability is insufficient for telecom requirements over more than 500 m distances, so that FSO links were more and more replaced by fiber and microwave links. Because small cells are located between the macro-cells, distances are shorter and, in this use case, the availability of optical links becomes higher. Enhanced availability is required in general for tighter interference coordination, despite the fact that availability requirements in the access link of small cells can be smaller, as the mobile terminal is covered by the macro-cell in parallel.

Robustness against alignment errors is regarded as a second main objective. Laser light has a collimated Gaussian beam shape, i.e., solid mounting of FSO equipment at the transmitter and receiver end is mandatory. Base stations at lamp or telegraph masts are commonly used in some areas and considered outdoors also for small cells. Obviously, rectangular instead of Gaussian beam shape is an appropriate solution. In [8], laser light is first coupled into a multimode fiber (MMF). After propagation through the MMF, the light develops a homogeneous beam profile with a random Speckle pattern. An image of the MMF output is formed at the receiver, where a lens then focuses the received light onto a photodiode. Multiple overlapping beams are used in [8] to average out the fading. However, the complexity is higher.

Lowering the cost is considered as a third main objective. A wireless link should cost less than digging the fiber. Typical digging costs represent almost 50% of the total costs for a fibre-to-the-home deployment [9]. The use of light-emitting diodes (LEDs) is promising to reduce cost. The 10 Mb/s RONJA link [10] used an LED from a car brake light and a 13 cm lens to create a 4 m spot diameter at 1 km distance, which makes alignment easy. Materials costs are low, details are publicly available while manufacturing of the link is time-consuming. The 1 Gb/s KORUZA link [11] follows classical FSO design paradigms. To reduce costs, a bidirectional small-form pluggable (SFP) single-mode fiber transceiver is used. Manufacturing details are publicly available and mechanical parts can be obtained using a 3D printer. At 100 m distance, however, the spot has 1 cm diameter only and it has to be manually tracked to hit the receiver lens. Stepper motors are used next to align the SFP module inside the device to track the narrow laser beam automatically and to reduce residual alignment error. Almost the entire link margin of the SFP module is available in this way to overcome impairments, as the spot falls fully inside the receiver lens. Obviously the initial alignment to hit the lens with a narrow beam is a challenge.

Altogether, the objectives of the present paper are to develop a robust, easy-to-align and low-cost optical wireless link capable to address the needs of outdoor deployment of modern small-cell mobile radio technologies, like IEEE 802.11 (WiFi) and LTE, and to realize both, high data rate (200 Mb/s over around 200 m) and low latency (few ms). Our new approach is based on previous work on high-speed visible light communications (VLC) [1], [11]. In order to address the need for low cost, a high-power infrared LED (55 mW) and a large-area photodiode (1 cm^2) are used at the transmitter and receiver, respectively. The bandwidth of both components was increased to more than 150 MHz using sophisticated driver and transimpedance amplifier (TIA) circuits. Similar like in the RONJA link, alignment is very easy. But the wide beam implies a significant path loss so that no link margin is available. Robustness against bad weather conditions is therefore added using rate-adaptive transmission, as suggested in [13]. It has been realized using a commercial discrete multitone (DMT) chipset adapting the data rate in real-time, based on feedback information provided over the reverse link.

Major achievements are a first experimental setup with which initial outdoor field trials were conducted, a mathematical model of the link including the major impairment effects due to the fog and the sunlight, an optimized link design, the setup of an optimized prototype using latest DMT technology and the proof-of-concept that the targeted data rates can be achieved at low latency despite the inherent delay caused by introducing real-time rate-adaptive digital signal processing.

The paper is organized as follows. In Section II, a mathematical model of the optical wireless link including the main impairments is presented. In Section III, the experimental prototype and the field trial setup are described. In Section IV, field trial results, the optimized link design and initial proof-of-concept results with the optimized prototype are reported. In Section V, the potential of OWC towards the deployment of future 5G mobile networks is discussed.

II. Mathematical Model of the Optical Wireless System With Impairments

A system model for the optical wireless link is described in this chapter, to include the role of the transmitter, the receiver, as well as the impact of weather impairments onto the channel.

On the transmitter side, the LED and the lens are modeled yielding the optical beam characteristics. Next, the optical channel is included with path losses due to the propagation and the fog. Finally, the lens and the receiver noise are modeled including the effect of sunlight. From the model, an electrical signal-to-noise ratio (SNR) can be obtained. Together with the bandwidth and an implementation penalty, the achievable data rate is estimated using Shannon's formula.

A. Transmitter

The transmitter is described by the size of the used infrared LED and the collimating lens resulting in the divergence half angle Θ/2

$$\Theta/2 = \arctan\left(0.5 \cdot (d_{\mathrm{LED}} - d_{\mathrm{Beam},f_t})/f_t\right), \tag{1}$$

where d_{LED} is the LED diameter and f_t the focal length of the transmitter lens. By knowing f_t and d_{LED} and assuming that the beam diameter $d_{\mathrm{Beam},\,ft}$ in the focal point is zero, Θ/2 can be calculated. Note that the LED beam characteristics and the transmitter lens diameter d_t have to be matched so that most of the emitted optical power can be captured and collimated towards the receiver. Our calculations include a loss of 20% of the optical power due to inaccuracy and component tolerances. Based on Θ/2 and d_t, the spot diameter d_S at the receiver can be calculated as

$$d_S(L) = d_t + 2 \cdot L \cdot \tan(\Theta/2), \tag{2}$$

where *L* is the transmission distance. The spot diameter is needed in the following subsection for calculating the geometrical loss.

B. Optical Channel

The optical channel is described by the power loss of the light while traveling through the atmosphere and being received by the photodiode. Although anti-reflection-coated, the lenses used to collimate the LED light and to focus it on the PD have less than 100% transmittance. Therefore, transmittance of 0.9 corresponding to a loss of roughly 1 dB is assumed in the model. Using a waterproof housing with an acrylic glass front yields an additional 1.5 dB path loss. Thus the resulting optical losses amount to

$$G_{\mathrm{opt}} = 2.5\ dB. \tag{3}$$

Due to the enlarged optical spot caused by the transmitter divergence and the limited area of the receiving lens, only a fraction of the transmitted optical power is focused onto the PD. The corresponding geometrical loss G_{geom}

$$G_{\mathrm{geom}} = 10\log\left(d_r/d_s(L)\right)^2 \tag{4}$$

depends on the receiving lens diameter d_r, and the enlarged spot size d_S at the receiver, see (2).

While travelling from the transmitter to the receiver, part of the light is attenuated due to aerosol and molecular absorption or scattering in the atmosphere. The corresponding attenuation is the atmospheric loss described using the Beer-Lambert law

$$\tau(\lambda, L) = P(\lambda, L)/P(\lambda, 0) = e^{-\gamma(\lambda)L}, \tag{5}$$

where λ is the wavelength of the light, *γ(λ)* is the total extinction coefficient per unit length, *L* the distance from the transmitter, while *P(λ,L)* and *P(λ,0)* are the transmitted and received powers. The visibility range V is an important parameter for calculating the attenuation due to atmospheric loss. It is defined as the distance at which a contrast value of 0.02 is attained, which is the smallest contrast perceivable for the human eye at 550 nm. Assuming the maximum visibility is limited due to this contrast, the extinction coefficient *γ(λ)* is

$$e^{-\gamma \cdot V} = 0.02 \rightarrow \gamma = 3.91/V. \tag{6}$$

The wavelength-dependent total extinction coefficient is included in the model of Kruse in the following form

$$\gamma(\lambda) = 3.91/V\,[\lambda/550]^{-q}, \tag{7}$$

where factor *q* describes the size distribution of scattering particles. The values for *q* can be obtained from Kim's model [14]

$$q = \begin{cases} 1.6 & \text{for V} > 50 \text{ km} \\ 1.3 & \text{for 6 km} < \text{V} < 50 \text{ km} \\ 0.16\,V + 0.34 & \text{for 1 km} < \text{V} < 6 \text{ km} \\ V - 0.5 & \text{for 0.5 km} < \text{V} < 1 \text{ km} \\ 0 & \text{for V} < 0.5 \text{ km}. \end{cases} \tag{8}$$

This model was validated against empirical data and it suggests that there is no wavelength-dependence of visibility below 500 m. Thus, the atmospheric loss is given by

$$G_{\mathrm{atm}} = 10\log\left(e^{-\frac{3.91}{V}\left[\frac{\lambda}{550}\right]^{-q}\cdot L}\right). \tag{9}$$

While scintillation is the most important turbulence effect for FSO systems, due to the locally varying refractive index in the atmosphere after interaction with solar energy, it can be neglected for short-range optical wireless links (< 500 m) [7].

Considering the above mentioned losses and knowing the transmitted power, the received power can be obtained as

$$P_R = P_T - G_{\mathrm{opt}} - G_{\mathrm{geom}} - G_{\mathrm{atm}}. \tag{10}$$

C. Receiver

Similar to the divergence of the light at the transmitter, the receiver shows a limited field of view (FOV) α_{FOV}

$$\alpha_{\mathrm{FOV}} = 2\arctan\left(0.5 \cdot d_{\mathrm{PD}}/f_r\right). \tag{11}$$

The FOV depends on the diameter of the photodiode (PD) d_{PD} and the focal length f_r of the receiving lens which enlarges the effective detector area of the PD. The FOV is not limiting the received optical power. In our experimental setup, it has no impact onto the alignment as it is larger than the divergence at the transmitter.

D. Noise Sources

Beside the losses occurring while the light is transmitted through the atmosphere, there are also impairments caused by noise at the receiver. There are two main noise sources. The first one is shot noise related to the discrete nature of carriers (i.e., electrons and holes) in the p-n junction of the photodiode resulting in current fluctuations. Shot noise has a quantum nature. Its mean-square noise current (variance) over a spectral range $\Delta\lambda$, which is the system bandwidth, is given by

$$\overline{i^2_{\text{shot}}} = 2eI\Delta\lambda \Rightarrow U^2_{\text{shot}} = 2eI\Delta\lambda R_L, \tag{12}$$

where e is the elementary charge, I the photocurrent and R_{L} the transimpedance of the amplifier. Shot noise can be approximated by a Gaussian distribution in case of high light intensity, with a variance equal to the mean square noise current stated above. In addition to the photocurrent, due to received modulated light, the background radiation has to be considered. The sum of all sources yields the total shot noise at the receiver. Under normal conditions, the background radiation is induced by sunlight, and it has only a negligible influence on the system performance. But in case of a large FOV at the receiver, it can be significant, due to strong sunlight, as observed in Section IV. By using an optical band-pass filter, distortion sue to the sunlight can be reduced. For the following calculations, a maximum background radiation of 2 $\text{Wm}^{-2}\cdot\text{sr}^{-1}\cdot\text{nm}^{-1}$ [16] is assumed.

Next to the shot noise, there is the thermal noise of the PD, the noise induced by the PD amplifier and the thermal noise due to the feedback resistor of the amplifier. Depending on what amplifier design is chosen, one of the above noise sources is dominant. For the transmission at high data rates, a high receiver bandwidth is needed, which can be further improved by introducing a peaking in the gain of the amplifier at the cut-off frequency. Next to the so realized cut-off frequency enhancement, the noise in the amplifier becomes dominant compared to the PD noise, which is then negligible [15]. The amplifier noise is given by

$$U^2_{n,\,\text{amp}} = \left(U_{\text{nif}}/f_{n,\,\text{peak}}\right)^2 \cdot \left(f^3_{n,\,\text{peak}} - f^3_z/3\right), \tag{13}$$

where U_{nif} is the voltage amplifier input noise, f_z and $f_{n,\,\text{peak}}$ are the start and stop frequencies of the rising edge of the introduced noise peaking. The amplifier noise induced by an increased voltage and current noise starts to be dominating all other noise sources at

$$f_{n,\,\text{peak}} = \left(1/2\pi U^2_{n,\,\text{amp}} C_{\text{PD}}\right) \cdot \sqrt{2eI + i^2_{n,\,\text{amp}} + 4k_B T/R_f}, \tag{14}$$

where C_{PD} is the capacitance of the PD, $i^2_{n,\,\text{amp}}$ the amplifier current noise, k_{B} the Boltzmann constant, T the temperature and R_f the feedback resistor of the amplifier. In addition, the thermal noise of the PD and the thermal noise due to the feedback resistor of the amplifier have to be considered

$$U^2_{\text{term,\,PD}} = I_{\text{dark}} \cdot R_L, U^2_{\text{term,\,Rf}} = 4k_B T/R_f, \tag{15}$$

with I_{dark} being the dark current of the PD. The total noise voltage can be calculated as follows:

$$U^2_{\text{noise}} = U^2_{n,\,\text{amp}} + U^2_{\text{term,\,Rf}} + U^2_{\text{shot,\,back}} + U^2_{\text{term,\,PD}}, \tag{16}$$

where $U^2{}_{\text{shot,back}}$ is the shot noise induced by the background radiation. As a metrics for the link quality, the electrical SNR is used, which is calculated as the ratio of the square of the signal voltage and the square of the total noise voltage [16]

$$\text{SNR} = U^2_{\text{signal}}/U^2_{\text{noise}}. \tag{17}$$

With the calculated SNR at the receiver and at a given bandwidth B, the maximum achievable throughput can be calculated according to Shannon's theorem. However, this needs to be done carefully.

First, the intensity-modulation direct-detection (IM/DD) channel requires a real-valued, non-negative waveform. If a bias current is added to the modulation signal and the modulation current is small compared to the bias current, the IM/DD channel can be modeled as a real-valued Gaussian channel having the throughput:

$$D_{\text{IM/DD}} = B/2\log_2\left(1 + \text{SNR}/\beta\right). \tag{18}$$

It should be noted that the throughput has to be divided by two in comparison to the classical form of Shannon's formula because of the real valued channel. A fixed empirical factor β is introduced, yielding an effective electrical SNR, in order to include implementation-related penalty due to the reduced modulation current, the imperfect frequency-selective link adaption together with non-ideal channel coding [17] or minor impairment effects not included in the model, yielding altogether a practical formula (18) for the achievable throughput. Note that (18) is no longer the capacity but the achievable throughput over the link. By including β, the throughput predicted by the link model can be matched to the data rate achieved over the experimental link, see Section IV.

III. Experimental Setup

A. Initial OW Link Setup

A real-time optical wireless (OW) system with 500 Mb/s peak gross data rate was implemented and used for initial outdoor tests. This initial link was derived from a previous setup described in [1], [12] by using different lenses to allow transmission over longer distances. A low-cost infrared LED SFH 4783 with a semiconductor area of 1×1 mm^2 was used as a light source. With an optical concentrator on top of the LED, the effective area is increased to 7×7 mm^2, yielding 25° divergence at full-width at half-maximum (FWHM) of the power. The transmitter was further equipped with a lens having 100 mm focal length and 3 inch diameter to reduce the beam-width down to 4° FWHM. At 100 m distance, the lens creates a 1000× increased image of the effective LED area, which enables a homogenous illumination representing a striking benefit for LED-based links. Due to the rectangular beam profile, alignment is simpler than in conventional FSO links using a Gaussian beam profile. On the other hand, the 7×7 m^2 spot at 100 m distance implies a

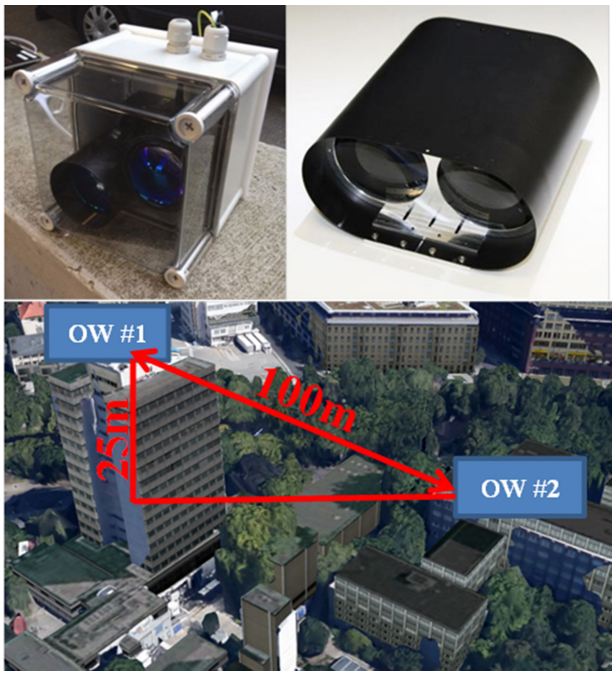

Fig. 2. Top left: Optical wireless transceiver prepared for outdoor trials, top right: optimized optical wireless system. Bottom: Campus map of TUB where the link is installed for long-term measurements (source Google Earth/Berlin 3D).

relatively large geometrical loss. At the receiver, a lens with f = 85 mm and 3 inch diameter was used in combination with a silicon photodiode S6968 from Hamamatsu having a 14 mm diameter. The receiver FOV is 9° and thereby larger than the beam divergence at the transmitter.

The 500 Mb/s OW link was deployed in an outdoor scenario, in order to conduct long-term measurements. Distance was 100 m and there was a difference of 25 m in height, like in a realistic macro-to-small-cell link scenario, revealing typical effects described in Section IV. Optical frontends were encapsulated in a weather-proof housing (see Fig. 2, top left).

Next to the outdoor link, a visibility sensor and weather station (Vaisala PWD12) was used to obtain statistical results concerning the impact of variable weather conditions onto the data rate. The visibility range (up to a maximum of 2000 m) and all types of precipitation were recorded every 2 minutes. Both systems, the initial and the optimized link described in the next subsection, were equipped with an add-on telescope in order to simplify the alignment. The telescope can be removed after the link is installed in order to save costs. In our measurements, an OFDM waveform with 70 MHz signal bandwidth was used. A known preamble is transmitted over the atmosphere and analyzed at the receiver to estimate the channel frequency response. After equalization at the receiver, the SNR per subcarrier is obtained. This information is sent back to the transmitter where the bit loading is adapted according to such feedback information. The overall possible gross data rate is than calculated by multiplying the bits per carrier with the respective bandwidth of the carrier and then adding all actual carrier data rates. When the channel conditions change, e.g., due to bad weather conditions like rain, fog or sunlight, the SNR per subcarrier is reduced and the bit loading at the transmitter yields a reduced data rate, while a pre-defined target for the bit error rate is maintained ensuring a robust link. Note that it is state of the art to use Ethernet in the mobile backhaul. I.e. the user data is obtained via Ethernet from the mobile network, converted to the adaptive DMT waveform, transmitted over the optical channel, received and decoded from the DMT signal so that the original Ethernet packets are retrieved and delivered to the small-cell base station.

B. Optimized OW Link Setup

After optimizing the link according to the model described in Section II, measurements were also conducted using an optimized OW link prototype. A new baseband chip with 100 MHz bandwidth, 1 Gb/s peak gross rate and a modified optical design were implemented in the new OW link. A much smaller LED SFH 4451 with a 0.3×0.3 mm^2 semiconductor area was chosen, additionally equipped with a parabolic reflector to enlarge the effective LED area to 1.8 mm^2 and to reduce the FWHM to 17°. Using 4 inch lenses with 166 mm focal lengths both at the transmitter and the receiver, a divergence of 0.26° and a FOV of 2.4° were realized, respectively. In this way, the emitted optical power has been reduced by a factor of 8 while the received optical power was simultaneously increased, as compared to the initial OW link.

IV. Results

A. Long-Term Measurement

To validate the link model and to get statistical results for the visibility range and the data rate in a realistic scenario, a long-term measurement was performed with the initial OW link during the winter term (end of November 2014 to end of April 2015) where challenging weather effects occurred like fog, rain and snowfall. Moreover the influence of direct or scattered sunlight was observed and described in this section.

In Fig. 3, the empirical cumulative distribution functions (CDF) of both, the visibility (top) and the data rate (bottom) of the OW link are shown. The CDF shows how often a quantity is smaller than the value plotted as the abscissa. For example, a visibility of 1 km with a CDF value of around 0.0085 indicates that the visibility was more than 1 km in 99.15% of all values measured during the whole 5-month period over the winter term. It should also be noticed that the visibility was never below 180 m. Moreover, it was higher than 2 km in 97.6% of all cases, indicating that the weather conditions were convenient most of the time during the measurement period. Our results in Fig. 3 (bottom) show in addition that the data rate was higher than 100, 39, 22 and 6 Mb/s in 72, 99, 99.9 and 100% of all cases. Obviously there was no link outage during the whole period, despite the challenging weather conditions.

Theoretically, a clear sky and the sun outside the FOV result in a negligible background noise at the receiver. Our model presented in Section II takes the sunlight into account only by assuming a background radiation of 2 $\mathrm{Wm^{-2}sr^{-1}nm^{-1}}$, which corresponds to bright sunlight. However, on some days in the

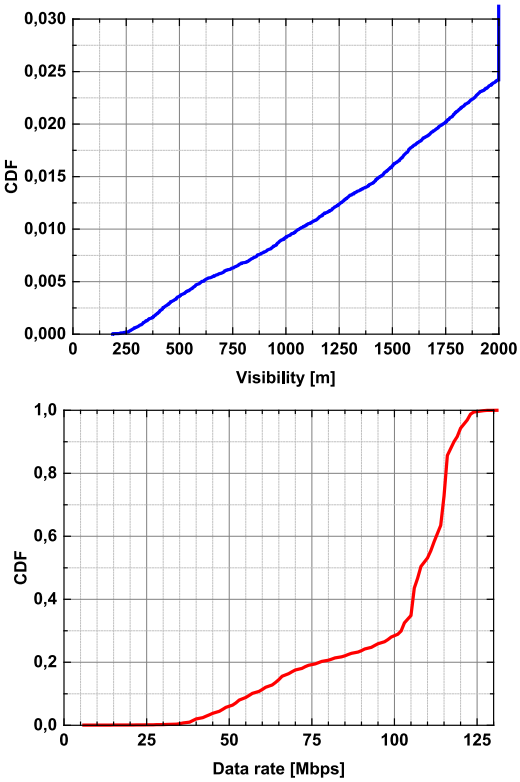

Fig. 3. Cumulative distribution function (CDF) of the visibility (top) and the measured data rate with the basic OW link (bottom) during the whole measurement period.

recorded statistics, the angle of incidence of the sun was very small. While the downward link pointed towards the south, a direct focus of the sunlight on the PD and the corresponding distortion were not observed. On the other hand, it was observed that a partly cloudy sky, back-illuminated by the sun, is likely to impair the link temporarily, as it generates noticeable background radiation at the receiver due to the scattered sunlight collected in the FOV. A corresponding exemplarily event, recorded between 1:00 a.m. and 5:00 a.m. on February 18, 2015, is shown in Fig. 4, where a reduction of the data rate is observed due to the reduced visibility range. Despite consistently high visibility after 7:00 a.m., data rate degrades gradually in particular between noon and 3:00 p.m.. The reduced link performance coincides with the sunrise at 7:15 a.m., in combination with a cloudy sky, resulting in certain intensity of the scattered sunlight. Only after the sunset at 5:24 p.m., the data rate returns to its maximum value.

While the steep rise of the data rate in the measured CDF in Fig. 3 can be explained by the visibility statistics, the tail towards lower data rates indicates that scattered sunlight disturbs the link. Note also that the distortion was observed simultaneously in both link directions. This observation can be explained by the urban environment, where, e.g., nearby the buildings, reflected or scattered sunlight falls inside the FOV at the receiver. The effect of diffusely reflected sunlight suggests the use of a reduced FOV at the receiver, as well as spectral filtering in the optimized OW link.

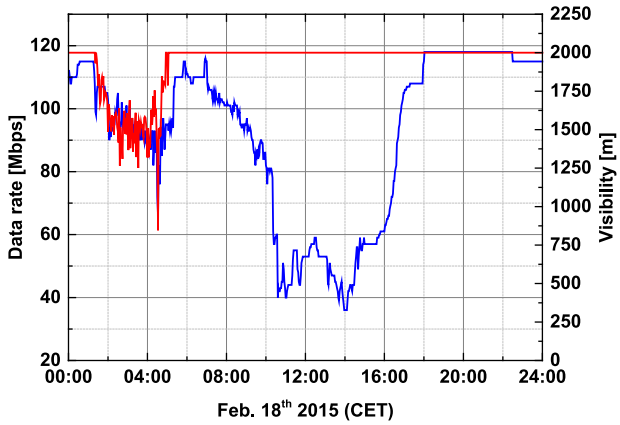

Fig. 4. Despite high visibility (red curve, top) reduced data rates for the OW link (blue curve, below) are observed for several hours due to sunlight scattered by clouds.

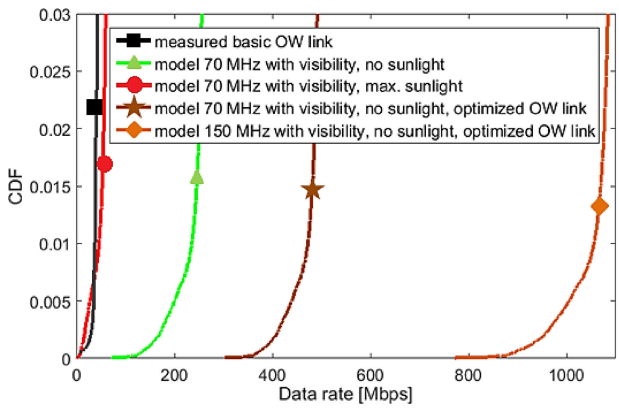

Fig. 5. Model-based CDF of the data rate for the basic and the optimized OW link over a distance of 100 m with and without sunlight and various system parameters, compared to measurement results.

Despite the variable weather conditions, the dynamic, closed-loop rate adaptation enabled an uninterrupted service for more than 5 months. Accordingly, our long-term measurements proof that a very high availability can be achieved over short optical wireless transmission distances of around 100 m.

B. Model Validation

In order to optimize the link design, the system model developed in Section II was used to modify the link parameters aiming at data rates of 1 Gb/s at 100 m. In Fig. 5, measured and calculated CDF results are compared.

Therefore, the data rate was first modeled by inserting the visibility range that was measured in each time interval into the link model. By calculating the atmospheric losses with the measured visibility range, the received optical power is predicted by the model. The received optical power and the model, considering also the implementation penalty using factor β, are than fed into the formula (18) to predict the SNR at the receiver and to obtain the achievable throughput. Note that a factor of $\beta = 15$ dB is used in (18). The largest contribution comes here from the

TABLE I
MODEL PARAMETERS OF THE INITIAL AND OPTIMIZED/IMPLEMENTED SYSTEM

	Parameter	Initial Value	Optimized/ Impl. Value
Link	Distance	100 m	100 m
	Wavelength	850 nm	850 nm
	Transmitter Lens Diameter	75 mm	100 mm
Transmitter	Focal Length Transmitter	100 mm	175/166 mm
	LED effective Diameter	7 mm	1.5 mm
	LED Half Angle	12°	15°/17°
	Radiant Flux	430 mW	50/55 mW
	Focal Length Receiver	85 mm	200/166 mm
	Receiver Lens Diameter	75 mm	100 mm
Receiver	Photodiode effective Diameter	14 mm	14 mm
	Dark Current	500 pA	500 pA
	Bandwidth	70 MHz	70/100 MHz
	Capacitance	50 pF	50 pF
T.I.A.	Feedback resistor	10 kΩ	1 kΩ
Optical Loss	Lens Transmittance	0.92	0.92
	Housing Transmittance	0.8	0.8
Ambient Light	Spectral Background Radiance	2 $Wm^{-2}sr^{-1}nm^{-1}$	2 $Wm^{-2}sr^{-1}nm^{-1}$

modulating current, whose amplitude was much smaller than the bias current so that the effects of clipping and non-linear LED characteristics were minimized and error-free DMT transmission was achieved. Moreover, there is an implementation loss due to the non-ideal frequency-selective link adaptation and the channel coding, which amounts to around 4 dB in a similar signal processing chain using LTE [17]. Background radiation caused by the scattered sunlight is included using minimal and maximal expected values.

In Fig. 5, the calculated CDF for the initial OW link is shown with no sunlight (green curve). Note that only the beginning of the CDF up to around 3% can be modeled and compared to the measurement because the visibility statistics ends at 2 km, due to limitations of the sensor used in experimental setup. Even if the factor β is included, there is no match between the calculated CDF without sunlight and the measured CDF. Only if the maximal distortion due to the sunlight is included (see Fig. 5, black curve), a significantly better match is achieved between measurement and model. This observation is consistent with the above statement that the tail in the measured CDF towards low data rates in Fig. 4 can be attributed to the sunlight. After matching the model to the initial OW link, the model is next used to modify the link parameters in the setup in order to optimize the performance, aiming at a data rate of 1 Gb/s over 100 m.

C. Link Optimization

In a first phase, the optimization aimed at increasing the data rate by varying optical parameters such as the effective diameter of the LED, the focal length at the transmitter and receiver and the lens diameters. Practical limits were thereby taken into account, since implementation was targeted as a final step. Table I shows the values used for the initial OW link and reasonable results for these optimized parameters.

As suggested by the model, reducing the radiating area of the LED from 7×7 mm^2 to 1.5×1.5 mm^2 and increasing the focal length of the transmitter lens from 100 to 175 mm result in a significantly reduced geometrical loss. Moreover, receiving lens area is almost doubled. In this way, despite having significantly less transmitted power, a higher received optical power is realized. The FOV is reduced simultaneously by increasing the focal length at the receiver. As an overall impact of these improvements for the optical design, and as a first result for the optimization, the electrical SNR has been increased by 26 dB. The calculated throughput of the optimized system is shown in Fig. 5 (brown curve). However, although the electrical SNR has been improved by a factor of 400, the data rate is only doubled, approximately. This is easily understood from formula (18). Because SNR is quite high, further increasing it is not adequate to achieve a significantly increased data rate because Shannon's capacity grows only with the logarithm of the SNR.

In a second phase, accordingly, the most relevant parameter in (18) has been increased, which is the bandwidth of the OW system, as it increases the data rate linearly. By using a hypothetic baseband signal processing exploiting the more than 150 MHz optical bandwidth offered by our LED driver [1] and a smaller PD, the model predicts that 1 Gb/s can be achieved over 100 m including the measured visibility statistics, and excluding the impact of sunlight, see Fig. 5 (orange curve). In practice, the influence of the sunlight can be reduced significantly, by adding an optical bandpass filter and a sunshade at the receiver. Moreover, the FOV can be further reduced by using a pinhole and eventually, also a longer focal length at the receiver lens. We believe that the impact of background radiation becomes negligible in this way.

D. Data Rate and Latency Measurements

While the optimization in the previous paragraphs indicated possible directions for a significantly higher data rate, practical limits of commercially available components have been taken into account for the realization of a new OW link. Table I summarizes the most significant system parameters both for the initial, as well as the optimized OW link. Note that the size of the PD was left unchanged because it would imply significant changes in the receiver electronics. Besides an optics redesign to achieve higher SNR, the key step was the introduction of a new baseband signal processor. The chip is a commercially available DMT baseband processor normally used for wired communication. It offers a baseband bandwidth of 100 MHz and a peak gross data rate of nearly 1 Gb/s in an electrical back-to-back configuration. This is achieved with a very effective bit and power loading in combination with high spectral efficiency modulation formats up to 12 bit/s/Hz. However, the frequency response of the analog optical frontends was carefully optimized so that a large fraction of the throughput was also achieved in the optical back-to-back configuration, see [18].

In Fig. 6, top, the measured data rate of the initial and the optimized OW systems are shown for different transmission distances to quantify the overall effect of the new link parameters. In the measurements, both links were mounted on movable platforms equipped with portable power supplies, enabling measurements with more than 200 m distance. By using the

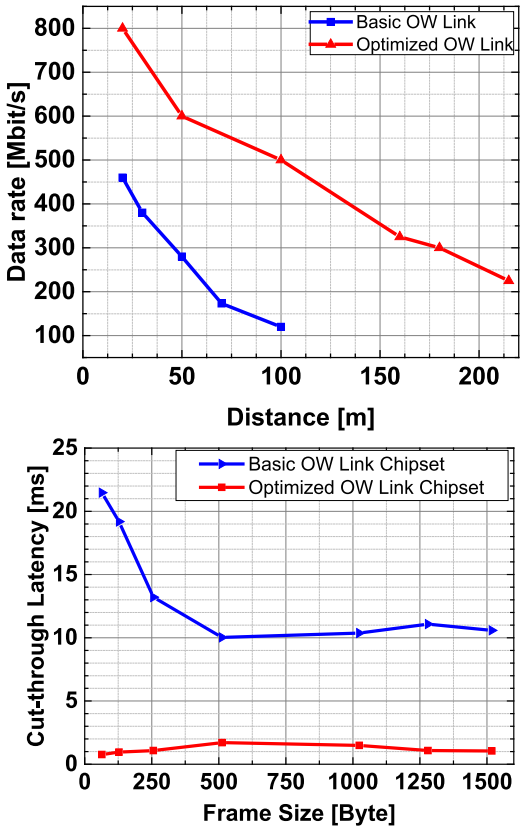

Fig. 6. Data rate as a function of transmission distance for the basic and optimized system (top), latency as a function of frame size (bottom).

monitoring tool of the used baseband chip, the maximum gross data rate at the physical layer of the baseband chip was measured after establishing a stable link between two OW modules by aligning them with the add-on telescopes. At 20 m distance, both the initial and the new experimental systems reach their practical maximum data rate of 465 and 800 Mb/s, respectively. At 100 m distance, the basic and optimized system achieved a gross data rate of 120 and 500 Mb/s, respectively. With the new link, the data rate is enhanced by more than a factor of 4x compared to the initial OW link. Even at 215 m distance, the optimized system still achieved 225 Mb/s. Assuming that a 4G LTE small-cell base station with 2×2 MIMO and 20 MHz bandwidth achieves a peak data rate if 150 Mb/s, if operated in a scenario free from inter-cell interference, e.g., by using a separate carrier frequency and a sufficient distance from other small cells using the same carrier frequency, with the new OW backhaul link, data rates are sufficient.

Furthermore, the fast link adaptation and handover in LTE require that low latency is also realized over the backhaul link, despite the rate-adaptive digital signal processing which has been introduced here in order to improve the robustness in variable weather conditions [18], [19]. Therefore, the average cut-through latency (i.e., end-to-end one-way) was measured using the standard RFC 2544 test. Results are shown in Fig. 6, bottom, as a function of the frame size at 95% traffic load. Besides offering a significantly higher data rate, the new baseband chip offers a significantly reduced latency of around 2 ms, which is also independent of the frame size.

A major reason for the reduced latency is that the new baseband chip supports instantaneous selective retransmission of lost data units already inside the physical layer. While the values achieved here are more than sufficient for LTE, fast retransmissions appear essential to achieve the latency requirements in future 5G networks. Altogether, while our results on the optimized link are only preliminary, they illustrate the potential of OW links in current and future mobile radio systems.

V. Discussion

The data rates achieved in the present paper indicate that low-cost optical wireless links, based on high-power infrared LED and large-area photodiodes, in combination with rate-adaptive transmission concepts, can satisfy already today essential requirements of high availability, sufficient data rates as well as low latency [18]–[22] for the use as an economic wireless backhaul technology for small cells that are needed to boost the performance in the current 4G mobile networks.

Towards the use in 5G networks, it is certainly essential to increase the data rates, however, small cells will most likely be connected via fronthaul, rather than backhaul technologies in order to enable tighter interference coordination controlled by the nearest macro cell. In order to facilitate rapid deployment, fronthaul may be implemented frequently using wireless technologies. In that case, it becomes obvious that new fronthaul technologies, based on Ethernet and the modified functional split, as explained in the Introduction, play a crucial role in order to minimize the required data rates. Nevertheless, connecting a small cell in 5G may need data rates in excess of 10 Gb/s.

The model of the optical wireless link developed in the present paper clearly shows into what direction the technology has to be developed in the near future. Data rate can best be increased by increasing the bandwidth of the optical wireless link, rather than the SNR, while maintaining the benefits of adaptive transmission in variable weather conditions. Over the short distances considered for small cells, we assume that an optical bandwidth of 1–2 GHz will be sufficient, which can only be reached by using lasers today. Note that low-cost high-power laser diodes which can be modulated at high speed are commercially available from DVD writers. What should also be maintained from the work presented here is the rectangular beam profile to simplify the deployments.

Note that a main reason for the reduced latency in Section IV is that the new chip supports a selective retransmission of lost data packets in the physical layer, i.e., nearly instantaneously. While the latency achieved here is more than sufficient for LTE, fast retransmissions over wireless feeder links may be an essential enabler to reach the latency requirements below 1 ms in future 5G networks.

VI. Conclusion and Outlook

In this paper, the new concept of a low-cost optical wireless links for the back- and fronthaul of small radio cells in

4G and 5G mobile network was introduced. The technology is based on LEDs as transmitters and photodiodes as receivers, in combination with rate-adaptive digital signal processing. By modification of an existing prototype, a first 5-month outdoor field trial has been conducted revealing the impact of variable weather conditions. It was found that the visibility range was never below 180 m, with 1 km in more than 99% of all times during the whole observation period. The use of rate-adaptive transmission improved the availability remarkably in the occasional presence of fog and sunlight.

A mathematical model of the backhaul link including these impairment effects has been presented and used to obtain an optimized link design. A prototype was implemented, accordingly, using optimized optics and a new 1 Gb/s baseband chip. With the much higher data rates of 800 to 225 Mb/s over distances of 20 and 215 m, respectively, and latency below 2 ms at 95% traffic load, it was demonstrated that, optical wireless communications can be used as a low-cost solution for the wireless backhaul of small mobile radio cells already today, e.g., for WiFi and LTE. Further development of the new concept proposed in this paper will be needed for the use also in future 5G mobile networks. While small cells may be connected via new fronthaul technologies in 5G, by using Ethernet and a modified functional split, higher data rates and reduced latency will both be needed. These targets can be achieved over a similar range of distances by increasing the bandwidth, e.g., using low-cost laser diodes, instead of LEDs, and further accelerating the digital baseband processing that is necessary for rate-adaptive transmission.

REFERENCES

[1] L. Grobe, A. Paraskevopoulos, J. Hilt, D. Schulz, F. Lassak, F. Hartlieb, C. Kottke, V. Jungnickel, and K.-D. Langer, "High-speed visible light communication systems," *IEEE Commun. Magazine*, vol. 51, no. 12, pp. 60–66, Dec. 2013.

[2] C. Bock, S. Figuerola, M.C. Parker, S.D. Walker, T. Mendes, V. Marques, V. Jungnickel, K. Habel, and D. Levi, "Convergent radio and fibre architectures for high-speed access," in *Proc. 15th Int. Conf. Trans. Opt. Netw.*, Jun. 2013, pp. 23–27.

[3] V. Jungnickel, K. Manolakis, W. Zirwas, B. Panzner, V. Braun, M. Lossow, M. Sternad, R. Apelfrojd, and T. Svensson, "The role of small cells, coordinated multipoint, and massive MIMO in 5G," *IEEE Commun. Mag.*, vol. 52, no. 5, pp. 44–51, May 2014.

[4] U. Dötsch, M. Doll, H.-P. Mayer, F. Schaich, J. Segel, and P. Sehier, "Quantitative analysis of split base station processing and determination of advantageous architectures for LTE," *Bell Labs Technical J.*, vol. 18, no. 1, pp. 1538–7305, 2013.

[5] N. J. Gomes, P. Chanclou, P. Turnbull, A. Magee, and V. Jungnickel, "Fronthaul evolution: From CPRI to Ethernet," *Opt. Fiber Technol.*, vol. 26, Part A, Dec. 2015, pp. 50–58.

[6] R. G. Hunsperger, *Photonic Devices and Systems*. New York, NY, USA: Marcel Dekker, 1994.

[7] A. Prokeš, "Modeling of atmospheric turbulence effect on terrestrial FSO link," *Radioengineering*, vol. 18, no. 1, pp. 42–47, Apr. 2009.

[8] CBL GmbH. (2015). [Online]. Available: http://www.cbl.de/23–0-AirLaser-IP1000-plus.html

[9] Fiber to the Home Council Europe, "FTTH Handbook," Edition 4.1, D&O Committee, 08/2011, p. 27

[10] Twibright Labs. (2015). [Online]. Available: http://ronja.twibright.com/

[11] Koruza project. (2015). [Online]. Available: http://koruza.net/index.html

[12] K.-D. Langer, J. Hilt, D. Schulz, F. Lassak, F. Hartlieb, C. Kottke, L. Grobe, V. Jungnickel, and A. Paraskevopoulos, "Rate-adaptive visible light communication at 500Mb/s arrives at plug and play," *Opt. Commun.*, SPIE Newsroom, 2013, doi: 10.1117/2.1201311.005196

[13] M. Karimi and M. Uysal, "Novel adaptive transmission algorithms for free-space optical links," *IEEE Trans. Commun.*, vol. 60, no. 12, pp. 3808–3815, Dec. 2012.

[14] I. I. Kim, B. McArthur, and E. Korevaar, "Comparison of laser beam propagation at 785 nm and 1550 nm in fog and haze for optical wireless communications," *Proc. SPIE*, vol. 4214, 2001, doi:10.1117/12.417512

[15] C. D. Philip Hobbs, *Building Electro-Optical Systems*. 2nd ed. Hoboken, NJ, USA: Wiley, 2009, pp. 688–698

[16] R. Ramirez-Iniguez, S. M. Idrus, and Z. Sun, *Optical Wireless Communications: IR for Wireless Connectivity*. New York, NY, USA: Auerbach, 2008.

[17] K. Manolakis, M. A. Gutierrez-Estevez, and V. Jungnickel, "Adaptive Modulation and Turbo Coding for 3GPP LTE Systems with Limited Feedback," presented at the IEEE 79th Veh. Technol. Conf., Seoul, Korea, May 2014.

[18] D. Schulz, M. Schlosser, C. Alexakis, K. Habel, J. Hilt, R. Freund, and V. Jungnickel, "Optical wireless LED link for the backhaul of small cells," presented at the OSA Technical Digest, Los Angeles, CA, USA, 2015, Paper M2F.8.

[19] D. Schulz *et al.*, "Low latency mobile backhauling using optical wireless links," ITG Fachtagung Breitband für Deutschland, Berlin, Germany, 2015.

[20] D. Schulz, C. Alexakis, M. Schlosser, J. Hilt, R. Freund, and V. Jungnickel, "Initial outdoor trials with optical wireless links for small-cell backhauling," in *Proc. ITG Symp. Photonic Networks*, Leipzig, Germany, May 2015, pp. 7–8.

[21] V. Jungnickel, D. Schulz, N. Perlot, K.-D. Langer, and W. Störmer, "Optical wireless as a low-cost small-cell backhaul solution," presented at the 9th ITG Symposium Broadband Coverage, Germany, Berlin, 1–2 Apr. 2014.

[22] V. Jungnickel, D. Schulz, J. Hilt, C. Alexakis, M. Schlosser, L. Grobe, A. Paraskevopoulos, R. Freund, B. Siessegger, and G. Kleinpeter, "Optical wireless communication for backhaul and access," presented at the European Conf. Optical Communication., Valencia, Spain, 2015, Paper We.3.4.1 (invited)

Dominic Schulz received the M.S. degree in communications engineering from Berlin University of Applied Sciences, Berlin, Germany, in 2012. Subsequently, he joined the Department of Photonic Networks and Systems, Fraunhofer Institute for Telecommunications, Heinrich Hertz Institute. He is currently working toward the Ph.D. degree in the field of optical wireless communications. His current activities include the development of high data rate systems for wireless access, as well as research toward long-range links.

Volker Jungnickel received doctorate and habilitation degrees from Humboldt University, Berlin, Germany, in 1995 and Technical University, Berlin, in 2015, respectively. In 1997, he joined the Fraunhofer Heinrich Hertz Institute, where he is leading the metro, access, and in-house systems group. He contributed to high-speed optical wireless links, a first 1 Gb/s mobile radio link, the first real-time trials of LTE and the first coordinated multipoint trials. He has contributed to 180 papers, 10 books, and 25 patents.

Christos Alexakis received the Diploma degree in electrical and computer engineering from the Democritus University of Thrace, Xanthi, Greece, in 2010 with specialization in Telecommunications and Space. In 2015, he received the M.Sc. degree in electrical engineering from the Technical University of Berlin, Berlin, Germany, with focus on the fields of optical communications and lighting engineering. From 2012 to 2015, he worked as a Scientific Assistant in the Department of Photonic Networks and Systems, Fraunhofer Heinrich Hertz Institute where he was involved in measurements of photonic components as well as in the research and development of Optical Wireless Communication Systems.

Michael Schlosser received the Diplom-Informatiker degree from the Technical University of Berlin, Berlin, Germany, in 2001. His diploma thesis was done at the Institute for Software Engineering and Theoretical Computer Science. In 2001, he joined the Photonic Networks Department, Fraunhofer Institute for Telecommunications Heinrich-Hertz-Institut and stayed there until 2015. He was engaged in different European IST-project (e.g., NOBEL phase I and phase II) and National research projects. Since 2016, he has been with the Berlin Institute for Software Defined Networks GmbH. His main research interests include optical networks, protocols for high speed networks and network optimization of communication networks.

Jonas Hilt received the Diploma degree in electrical engineering from Berlin University of Applied Sciences, Berlin, Germany, in 2009. In 2009, he joined the Fraunhofer Institute for Telecommunications, Heinrich Hertz Institute, where he is an Electrical Engineer in the Department of Photonic Networks and Systems. His current activities include the area of design and realization of embedded systems and visible light communication systems.

Anagnostis Paraskevopoulos received the degree in electrical engineering from the Technical University in Athens, Athens, Greece, and the Ph.D. degree from Université Paris-Orsay, Orsay, France, with a study on RF modulation of semiconductor lasers. He joined HHI in 1988 and has since been involved in various technology research projects. Over the years he has successfully coordinated R&D projects concerning both research subjects and industrial applications. He is an author and co-author of more than 50 scientific papers.

Liane Grobe received the Dipl.-Ing. degree in media technology from Technische Universitaet Ilmenau, Ilmenau, Germany, in 2008. From 2009 to March 2011, she was with the communication research laboratory at the same university, where her research tasks are directed on optical wireless data transmission systems. From April to September 2011, she joined the University of Applied Sciences Nordhausen, Germany, working on the topic of signal processing for fiber optical communication. In October 2011, she changed to the Photonic Network and Systems Department, Fraunhofer Heinrich Hertz Institute, Berlin, Germany. Her activities are mainly focused on digital signal processing for Visible Light Communication, then. Since November 2015, she has been with the P3 communications GmbH, Berlin, Germany.

Péter Farkas received the Diploma degree in communications engineering from the Technical University of Berlin, Berlin, Germany, in 2011. In his final thesis, he focused on the modeling of nonlinear effects in Semiconductor Optical Amplifiers. Since 2011, he has been working in the field of network design, modelling and planning at the Department of Photonic Networks and Systems, Fraunhofer Institute of Telecommunications, Heinrich Hertz Institute. His recent activities include integration of optical wireless communication into access networks.

Ronald Freund received the Dipl.-Ing. and the Dr.-Ing. degrees in electrical engineering from Technical University of Ilmenau, Ilmenau, Germany, in 1993 and 2002, respectively. In 2013, he received the MBA degree from RWTH Aachen, Aachen, Germany. Since 1995, he has been with the Heinrich Hertz Institute in Berlin, where he is currently leading the Department of Photonic Networks and Systems.